Kinetic Modeling of Aqueous and Hydrothermal Synthesis of Barium Titanate ($BaTiO_3$)

Andrea Testino,[†] Vincenzo Buscaglia,*[,‡] Maria Teresa Buscaglia,[‡] Massimo Viviani,[‡] and Paolo Nanni[†,‡]

Department of Process and Chemical Engineering, University of Genoa, I-16129 Genoa, Italy, and Institute of Energetics and Interphases, National Research Council, I-16149 Genoa, Italy

Received May 26, 2005. Revised Manuscript Received August 4, 2005

A rigorous kinetic model for the solution precipitation and hydrothermal synthesis of $BaTiO_3$ particles is proposed. Three elementary kinetic processes are considered: primary nucleation, secondary nucleation, and diffusion-controlled growth. Secondary nucleation accounts for the acceleration of the formation kinetics after an initial slow crystallization stage and the formation of $BaTiO_3$ particles with a polycrystalline substructure. The time evolution of yield, crystal size, and particle size is represented by means of discretized mass and population balance equations. The system is simulated by replacing the continuous particle distribution with a limited number of size classes. A modification of the discrete equation describing growth has allowed the simulation of diffusion-controlled growth. The properties of the system are obtained from the moments of the particle size distribution. A new algorithm capable of exactly calculating a generic number of moments has been developed. The model correctly describes the kinetic data for eight different experimental conditions, and the value of the adjustable parameters is consistent with the best physical estimates available. The present approach shows that knowledge-based synthesis of $BaTiO_3$ particles with tailored size and properties is possible, minimizing the need for trial and error experimentation.

1. Introduction

Barium titanate, $BaTiO_3$, is a ceramic material widely used in the electronics industry for the fabrication of multilayer ceramic capacitors (MLCCs), pyroelectric elements, heaters with a positive temperature coefficient of resistivity (PTCR), and embedded capacitance in printed circuit boards.[1] The continuous advance in microelectronics and communications is gradually leading to the miniaturization of MLCCs. Market trends indicate that, within a few years, the thickness of a single ceramic layer will be decreased below 1 μm.[2] To achieve this goal, powders composed of small particles (100−300 nm) with a narrow size distribution are required.

In recent years, there has been a growing interest in the hydrothermal method and, more generally, in solution precipitation methods for the production of high-quality submicron $BaTiO_3$ powders suitable for the processing of advanced MLCCs.[3−15] The thermodynamic modeling work of Lencka and Riman on hydrothermal synthesis has assessed the conditions corresponding to the formation of barium titanate.[16] In the absence of CO_2 and at pH > 12, $BaTiO_3$ is the stable solid phase over a wide range of barium concentrations and temperatures. The potential advantage of hydrothermal and related methods in comparison to other synthesis routes is the possibility to control the size of the final particles. The size distribution of particles that grow from a solution depends, in general, on the relative rates of nuclei formation and crystallite growth.[17] If the nucleation rate is high, the number of particles generated will be large while the size of the final particles will be relatively small. For a given system, the rates of nucleation and growth depend on supersaturation. Supersaturation is affected by reactant concentration, temperature, and mixing conditions. Thus, the final particle size distribution can be tailored by changing the synthesis conditions.[15]

* Corresponding author. E-mail: v.buscaglia@ge.ieni.cnr.it.
† University of Genoa.
‡ Institute of Energetics and Interphases, National Research Council.

(1) Rae, A.; Chu, M.; Ganine, V. In *Ceramic Transactions Dielectric Ceramic Materials*; Nair, K. M., Bhalla, A. S., Eds.; The American Ceramic Society: Westerville, OH, 1999; Vol. 100, p 1.
(2) Reynolds, T. G., III *Am. Ceram. Soc. Bull.* **2001**, *80*, 29.
(3) Vivekanandan, R.; Philip, S.; Kutty, T. R. N. *Mater. Res. Bull.* **1986**, *22*, 99.
(4) Gherardi, P.; Matijevic, E. *Colloids Surf.* **1988**, *32*, 257−274.
(5) Fukai, K.; Hidaka, K.; Aoki, M.; Abe, K. *Ceram. Int.* **1990**, *16*, 285.
(6) (a) Dutta, P. K.; Gregg, J. R. *Chem. Mater.* **1992**, *4*, 843. (b) Dutta, P. K.; Asiaie, R.; Akbar, S. A.; Zhu, W. *Chem. Mater.* **1994**, *6*, 1542. (c). Asiaie, R.; Zhu, W. D.; Akbar, S. A.; Dutta, P. K. *Chem. Mater.* **1996**, *8*, 226.
(7) Chien, A. T.; Speck, J. S.; Lange, F. F.; Daykin, A. C.; Levi, C. G. *J. Mater. Res.* **1995**, *10*, 1784.
(8) Kumazawa, H.; Annen, S.; Sada, E. *J. Mater. Sci.* **1995**, *30*, 4740.
(9) (a) Her, Y.-S.; Matijevic, E.; Chon, M. C. *J. Mater. Res.* **1995**, *10*, 3106. (b) Her, Y.-S.; Lee, S.-H.; Matijevic, E. *J. Mater. Res.* **1996**, *11*, 156.
(10) Leoni, M.; Viviani, M.; Nanni, P.; Buscaglia, V. *J. Mater. Sci. Lett.* **1996**, *15*, 1302.
(11) Pinceloup, P.; Courtois, C.; Leriche, A.; Thierry, B. *J. Am. Ceram. Soc.* **1999**, *82*, 3049.
(12) Lu, S. W.; Lee, B. I.; Wang, Z. L.; Samuels, W. D. *J. Cryst. Growth* **2000**, *219*, 269.
(13) Grohe, B.; Miehe, G.; Wegner, G. *J. Mater. Res.* **2001**, *16*, 1901.
(14) (a) Xu, H.; Gao, L.; Guo, J. *J. Am. Ceram. Soc.* **2002**, *85*, 727. (b) Xu, H.; Gao, L. *J. Am. Ceram. Soc.* **2003**, *86*, 203.
(15) Testino, A.; Buscaglia, M. T.; Viviani, M.; Buscaglia, V.; Nanni, P. *J. Am. Ceram. Soc.* **2004**, *87*, 79.
(16) (a) Lencka, M. M., Riman, R. E. *Chem. Mater.* **1993**, *5*, 61. (b) Lencka, M. M.; Riman, R. E. *Ferroelectrics* **1994**, *151*, 159.
(17) Dirksen, J. A.; Ring, T. A. *Chem. Eng. Sci.* **1991**, *46*, 2389.

10.1021/cm051119f CCC: $30.25
Published on Web 09/17/2005

Despite the potential interest, there are a few kinetic studies on the formation and crystallization of $BaTiO_3$ particles from aqueous solution and a comprehensive kinetic model is still lacking. Hertl[18] as well as Kutty and Padmini[19] measured the formation kinetics of $BaTiO_3$ from TiO_2 (either crystalline[18] or amorphous[19]) suspended in aqueous $Ba(OH)_2$, but the evolution of particle morphology was not investigated. Golubko et al.[20] studied the evolution of the Ba/Ti ratio of a titanium hydroxide gel obtained by the hydrolysis of titanium butoxide suspended in aqueous $Ba(OH)_2$. Walton et al.[21] performed a time-resolved, in situ neutron powder diffraction study and measured the crystallization kinetics of $BaTiO_3$ at 125−200 °C. The resulting crystallization curves displayed a sigmoidal shape and a significant induction time, ascribed to a dissolution-precipitation mechanism. Eckert et al.[22] and, more recently, Moon et al.[23] investigated both the macroscopic formation kinetics of $BaTiO_3$ and the morphological evolution of the system by transmission electron microscopy (TEM), although for a single experimental condition. The results show that the initial formation of barium titanate particles is dominated by a nucleation and growth process. Similar conclusions were also reported by MacLaren and Ponton.[24] In some of the previous studies,[18−23] a kinetic analysis was attempted by means of simple kinetic equations originally proposed for solid-state reactions. However, this approach suffers from a series of limitations. First, the application of some model equations, like the Johnson−Mehl−Avrami equation, to solution precipitation processes is questionable. Second, these equations have rigid boundary conditions and only provide one or two macroscopic kinetic parameters, which are not easily correlatable to fundamental physical parameters, like supersaturation, surface energy, and diffusion coefficients. Finally, the adopted models are generally unable to describe the complexity of the solution precipitation processes. Indeed, in most cases, the kinetic data could not be fitted by a single equation over the full conversion range. However, the distinction between different reaction mechanisms that would dominate at different times is likely to be a consequence of the inadequacy of the adopted models rather than a real feature of the investigated systems.

In this work, a general and more rigorous kinetic approach to the formation of $BaTiO_3$ particles by solution precipitation is presented. This approach is based on the fundamental equations describing nucleation, growth, and aggregation processes from solution, without the use of empirical relationships. Mass and population balances were properly taken into account to describe the evolution of the system. In Section 2, the theoretical framework of the kinetic model is developed. In Section 3, the results of the model are compared with experimental data. In Section 4, main conclusions about the hydrothermal synthesis and aqueous precipitation of $BaTiO_3$ are drawn.

2. Description of the Kinetic Model

2.1. Reaction Mechanism. In a recent study,[25] the formation kinetics of $BaTiO_3$ particles at 80−90 °C from dilute ($\leq$0.1 M) aqueous solutions of $BaCl_2$ and $TiCl_4$ at pH 14 were reported. The overall reaction can be written as

$$BaCl_2(aq) + TiCl_4(aq) + 6NaOH(aq) \rightarrow BaTiO_3(s) + 6NaCl(aq) + 3H_2O(l) \quad (1)$$

where (aq) denotes a salt in aqueous solution. The analysis of a large number of experimental data collected in different conditions of concentration, temperature, and Ba/Ti ratio strongly supports the existence of a unique reaction mechanism. Therefore, the kinetic model was specifically developed and tested on the basis of the observations made in the previous paper.[25] Nevertheless, the model is quite general as it makes use of system-independent population balance equations to describe the fundamental processes involved in precipitation and can be easily adapted to simulate the formation of $BaTiO_3$ in different conditions. For simplicity, the influence of nonideality of the solutions and of particle size on surface and thermodynamic properties was neglected.

Reaction 1 proceeds in two distinct steps: (i) the initial, rapid formation of a titanium hydroxide gel (THG) phase and (ii) a slower reaction between the THG phase and the Ba^{2+} ions in solution with the formation of crystalline $BaTiO_3$. As a result, the overall kinetics is controlled by the crystallization process. The sigmoidal shape of the kinetic curves and the TEM observations strongly support a nucleation and growth mechanism for the second step. The formation of a THG phase as the intermediate product during the synthesis of $BaTiO_3$ from Ba−Ti solutions has also been described for other combinations of reactants: Ti tetrabutyloxide and Ba acetate,[26] Ti isopropoxide and Ba acetate,[24] and Ti isopropoxide modified with acetylacetone and Ba acetate.[23] Therefore, the two-step reaction mechanism outlined above has to be considered as a general feature of the formation of $BaTiO_3$ by solution precipitation in alkaline conditions. Moreover, the same mechanism should also apply to the hydrothermal synthesis (T > 100 °C) of barium titanate when the THG suspension obtained by the addition of NaOH or KOH to an aqueous solution of $BaCl_2$ and $TiCl_4$ is used as the precursor[12,14] or when the amorphous titanium hydroxide is produced by hydrolyzing a titanium precursor in a $Ba(OH)_2$ solution[11,27] before the hydrothermal treatment. From this point of view, the distinction between solution precipitation (T < 100 °C) and hydrothermal synthesis (T > 100 °C) is unnecessary. According to the available

(18) Hertl, W. *J. Am. Ceram. Soc.* **1988**, *71*, 879.
(19) Kutty, T. R. N.; Padmini, P. *Mater. Chem. Phys.* **1995**, *39*, 200.
(20) Golubko, N. V.; Yanovskaya, M. I.; Golubko, L. A.; Kovsman, E. P.; Listoshina, M. B.; Rotenberg, B. A. *J. Sol.-Gel. Sci. Technol.* **2001**, *20*, 135.
(21) Walton, R. I.; Millange, F.; Smith, R. I.; Hansen, T. C.; O'Hare, D. *J. Am. Chem. Soc.* **2001**, *123*, 12547.
(22) Eckert, J. O., Jr.; Hung-Houston, C. C.; Gersten, B. L.; Lencka, M. M.; Riman, R. E. *J. Am. Ceram. Soc.* **1996**, *79*, 2929.
(23) Moon, J.; Suvaci, E.; Morrone, A.; Costantino, S. A.; Adair, J. H. *J. Eur. Ceram. Soc.* **2003**, *23*, 2153.
(24) MacLaren, I.; Ponton, C. B. *J. Eur. Ceram. Soc.* **2000**, *20*, 1267.
(25) Testino, A.; Buscaglia, M. T.; Buscaglia, V.; Viviani, M.; Bottino, C.; Nanni, P. *Chem. Mater.* **2004**, *16*, 1536.
(26) Hennings, D.; Rosenstein, G.; Schreinemacher, H. *J. Eur. Ceram. Soc.* **1991**, *8*, 107.
(27) Chen, H.-J.; Chen, Y.-W. *Ind. Eng. Chem. Res.* **2003**, *42*, 473.

literature,[26,28] the gel phase obtained by the hydrolysis of Ti salts at high pH is composed of entangled networks of polymeric chains of titanium hydroxides. The skeleton of the polymers corresponds to Ti atoms linked by bridging O atoms. Therefore, the formula unit of the THG phase can be indicated as $TiO(OH)_2$. Since Ba ions do not belong to gel-forming ions, it is not expected that they participate in the formation of the gel network. A more reasonable assumption is that Ba^{2+} ions are adsorbed at the surface or trapped in the pores of the network.[26] According to the thermodynamic calculations of Lencka and Riman,[16] the predominant aqueous species of titanium in alkaline conditions is $Ti(OH)_4$, whereas for barium, both Ba^{2+} and $BaOH^+$ species are important at pH > 12. Therefore, it is assumed that nucleation and growth of the perovskite can be represented by the reaction

$$Ti(OH)_4(aq) + Ba^{2+}(aq) + 2OH^-(aq) \rightarrow BaTiO_3(s) + 3H_2O(l) \quad (2)$$

and local equilibrium conditions are assumed to hold at the surface of the growing crystal. The equilibrium between Ba^{2+} and $BaOH^+$ is given by

$$Ba^{2+}(aq) + OH^-(aq) \rightarrow BaOH^+(aq) \quad (3)$$

With reference to reaction 2, the supersaturation can be defined as

$$S = \frac{[Ti(OH)_4][Ba^{2+}][OH^-]^2}{K_s} \quad (4)$$

where K_s, that is, the solubility product, is the reciprocal of the equilibrium constant of reaction 2 and the square brackets indicate a concentration in mol dm^{-3}. To develop a consistent description of the formation kinetics of $BaTiO_3$, it is essential to recognize that (1) reaction 2 does not represent the molecular mechanism of the formation of $BaTiO_3$, (2) the choice of reaction 2 is arbitrary and only dictated by convenience, and (3) the value of supersaturation is independent of the aqueous species considered in the precipitation reaction as long as local equilibrium conditions prevail at the solid/liquid interface. For instance, if reaction 2 is rewritten using the species $BaOH^+$ instead of Ba^{2+}, expression 4 for supersaturation can still be obtained by considering the additional reaction 3.

It is clear that the $Ti(OH)_4$ species (or any other soluble Ti species) must be supplied by dissolution of the THG phase. Lencka and Riman[16] have shown that the solubility of TiO_2 at pH > 4 is constant and rather small, $\approx 10^{-8}$ mol dm^{-3}. The dissolution process can be schematically represented by

$$TiO(OH)_2(gel) + H_2O(l) \xrightarrow{OH^-} Ti(OH)_4(aq) \quad (5)$$

Hydrolysis processes such as reaction 5 can occur by a two-step mechanism. The first step corresponds to the nucleophilic attack of the hydroxyl ion (which acts as a catalyst) on a terminal Ti atom (denoted as Ti^*) of the polymeric network[28] and detachment of a $Ti(OH)_4$ molecule. The second reaction step corresponds to the reaction between the negatively charged terminal oxygen (O^*) originated by the detachment of $Ti(OH)_4$ with a water molecule, which restores the hydroxyl ion. If this first reaction step is assumed to be reversible and rate-controlling, the dissolution rate of the THG phase can be written as

$$-\frac{d[Ti_{gel}]}{dt} = k_1[Ti^*][OH^-] - k_{-1}[O^*][Ti(OH)_4] \quad (6)$$

where $[Ti_{gel}]$ is the number of moles of titanium contained in the THG phase per unit volume of the reacting suspension and k_1 and k_{-1} are the kinetic constants of the direct and reverse process, respectively. If the terms $[Ti^*]$ and $[O^*]$ are assumed to be proportional to $[Ti_{gel}]$, eq 6 can be rewritten, after some manipulations, as

$$-\frac{d[Ti_{gel}]}{dt} = k[Ti_{gel}][OH^-]\left\{1 - \frac{K}{K_s}[Ti(OH)_4]\right\} \quad (7)$$

where k is the rate constant for THG dissolution and K is the reciprocal of the equilibrium constant of the overall reaction

$$TiO(OH)_2(gel) + Ba^{2+}(aq) + 2OH^-(aq) \rightarrow BaTiO_3(s) + 2H_2O(l) \quad (8)$$

The value of K can be determined from low-concentration experiments corresponding to nonquantitative precipitation of the perovskite. In this condition, $BaTiO_3$, the THG phase, and the solution coexist in equilibrium at the end of the reaction. It resulted in a value of $K = 1.05 \times 10^{-3}$ mol^3 dm^{-9} at 82 °C and $K = 8.18 \times 10^{-4}$ mol^3 dm^{-9} at 92 °C. By comparing reactions 2, 5, and 8, it can be easily shown that the ratio K_s/K represents the equilibrium solubility of the THG phase.

A mechanism similar to that depicted in the foregoing discussion can also be applied to the classical hydrothermal process, when crystalline titania is suspended in aqueous $Ba(OH)_2$. In such a case, the soluble Ti species will be provided by dissolution of TiO_2 particles and the dissolution rate will be proportional to the surface of titania.

2.2. Mass Balances. The mass balance for titanium in a closed system can be written as

$$-\frac{d[Ti_{aq}]}{dt} = \frac{d[Ti_{BT}]}{dt} + \frac{d[Ti_{gel}]}{dt} \quad (9)$$

where $[Ti_{aq}]$ is the overall concentration corresponding to all the aqueous titanium species (it practically corresponds to $[Ti(OH)_4]$). The amount of titanium precipitated as $BaTiO_3$ is $[Ti_{BT}]$. Concentration is always referred to the volume of the reacting suspension. The first term on the right-hand side of eq 9 corresponds to the formation rate of $BaTiO_3$ as a result of nucleation and growth events

$$\frac{d[Ti_{BT}]}{dt} = \{\hat{B} + \hat{G}\} \quad (10)$$

(28) Brinker, C. J.; Scherer, G. W. *Sol−Gel Science. The Physics and Chemistry of Sol−Gel Processing*; Academic Press: San Diego, CA, 1990.

where $\hat{B}$ and $\hat{G}$ are the nucleation and growth rate in mol dm^{-3} s^{-1}, respectively. The second term on the right-hand side of eq 9 corresponds to the dissolution rate of the THG phase, given by eq 7. Therefore

$$\frac{d[Ti_{aq}]}{dt} = k[Ti_{gel}][OH^-]\left(1 - \frac{K}{K_s}[Ti(OH)_4]\right) - \{\hat{B} + \hat{G}\} \tag{11}$$

This equation relates the formation rate of $BaTiO_3$ by nucleation and growth to the disappearance of the intermediate THG phase. If the Ba/Ti molar ratio in THG is denoted with R_{gel}, the mass balance for barium is immediately given by

$$\frac{d[Ba_{aq}]}{dt} = R_{gel}\frac{d[Ti_{gel}]}{dt} - \{\hat{B} + \hat{G}\} \tag{12}$$

where $[Ba_{aq}]$ is the overall Ba concentration corresponding to the sum of $[Ba^{2+}]$ and $[BaOH^+]$.

2.3. Population Balance. The population balance equation (PBE) or particle number continuity equation describes the evolution of the size distribution of an ensemble of particles simultaneously undergoing nucleation, growth, coalescence, and disruption. For a well-mixed suspension of constant volume, the population balance of the system can be written as[29]

$$\frac{\partial n(L,t)}{\partial t} + \frac{\partial}{\partial L}[G(L,t)\, n(L,t)] = B(n) - D(n) \tag{13}$$

where $n(L,t)$ is the number density of particles at time t in the size range L to $L + dL$ (for spheres with radius R, it is $L = 2R$), G is the isotropic growth rate, and B and D are the rates of birth and death, respectively. If there are dN particles per unit volume, the density function is $n = dN/dL$. Equation 13 relates the rate of accumulation of particles in the size range L to $L + dL$ to the microscopic particle growth rate and to the rate at which particles of that size are directly created or removed (birth and death processes). If disruption is neglected, the birth of new particles will be determined by nucleation and aggregation, whereas death will only occur by aggregation. In such a case, the contribution of aggregation can be written as[29]

$$B(L) = \frac{L^2}{2}\int_0^L \frac{\beta[(L^3 - \lambda^3)^{1/3},\lambda]\; n[(L^3 - \lambda^3)^{1/3}]\; n(\lambda)}{(L^3 - \lambda^3)^{2/3}} d\lambda$$

$$D(L) = n(L)\int_0^\infty \beta(L,\lambda)\; n(\lambda)\; d\lambda$$

where β is the aggregation kernel, a measure of the frequency of collisions between particles of size L and λ that are successful in producing particles of size $L + \lambda$. In general, β is a function of particle size. The moments of the size distribution are useful quantities in the solution of PBE problems. The jth moment can be defined as

$$m_j = \int_0^\infty L^j n(L)\, dL \tag{14}$$

The first four moments are of particular interest as they define the total number, length, surface, and volume of particles per unit volume of suspension by[29,30]

$$N_T = m_0 \tag{15a}$$

$$L_T = \epsilon_L m_1 \tag{15b}$$

$$A_T = \epsilon_A m_2 \tag{15c}$$

$$V_T = \epsilon_V m_3 \tag{15d}$$

where ϵ_L, ϵ_S, and ϵ_V are appropriate shape factors. It can be shown[29,30] that, for nucleation, growth at constant rate G (m s^{-1}), and aggregation, the PBE can be reduced to two ordinary differential equations

$$\frac{dm_0}{dt} = B_0 - \frac{1}{2}\beta_0 {m_0}^2 \tag{16a}$$

$$\frac{dm_3}{dt} = 3Gm_2 \tag{16b}$$

where B_0 is the nucleation rate (number density of particles per unit time, cm^{-3} s^{-1}) and β_0 is the aggregation kernel assumed to be independent of particle size. If β is a function of particle size, the second term on the right-hand side of eq 16a will have a more complex form. The above equations give, after integration, the total number of particles and the mean particle volume as a function of time. However, in the case of small particles ($<1\mu$m) like the $BaTiO_3$ particles of this study, the slip velocity of the particle with respect to the solvent is very small and growth is typically controlled by diffusion.[17] In this condition, eq 16b can be rewritten as (see Supporting Information)

$$\frac{dm_3}{dt} = 3G_0 m_1 \tag{16c}$$

and the growth rate is inversely proportional to the size of the particle,

$$\frac{dL}{dt} = \frac{G_0}{L} \tag{17}$$

The meaning of the term G_0 in eq 17 will be discussed later.

2.4. Discretization. The complexity of the general PBE can be overcome by the generation of discrete equations to replace the continuous differential eq 13. The discretization allows for a more efficient and simpler solution by use of conventional finite differences techniques. For this purpose, the system is simulated by replacing the continuous particle size distribution (PSD) by a limited number of classes. If N_i is the number of particles in the ith size class, the variation dN_i/dt can be split into the different contributions related to nucleation, growth, and aggregation

(29) Randolph, A. D.; Larson, M. A. *Theory of Particulate Processes. Analysis and Techniques of Continuous Crystallization*; Academic Press: San Diego, CA, 1988.

(30) Hounslow, M. J.; Ryall, R. L.; Marshall, V. R. *AIChE J.* **1988**, *34*, 1821.

$$\frac{dN_i}{dt} = \left(\frac{dN_i}{dt}\right)_{nucl} + \left(\frac{dN_i}{dt}\right)_{growth} + \left(\frac{dN_i}{dt}\right)_{aggr} \quad (18)$$

Expression 14 of the *j*th moment can be rewritten, in discrete form, by replacing the integral with a summation over the number of classes

$$m_j = \sum_i \overline{L_i^j} N_i \quad (19)$$

where $\overline{L_i^j}$ is the appropriate mean size in the *i*th class to calculate the *j*th moment and N_i is the number of particles in that class. The use of intervals with constant amplitude is, in general, not convenient, and the variable-step grid proposed by Lister et al.,[31]

$$\frac{L_{i+1}}{L_i} = 2^{1/3q} = r \quad (20)$$

where L_i and L_{i+1} define the extremes of the *i*th interval and q is a positive integer, was used in the model. It can be shown[30,31] that the mean values associated with this discretization grid are given by

$$\overline{L_i^j} = \frac{1}{j+1}\left(\frac{r^{j+1}-1}{r-1}\right) L_i^j \quad (21)$$

Discretization for Nucleation. Nucleation produces new particles of critical size L^* at rate B_0, which can be assigned to the relevant interval i_0. Therefore, the first term on the right-hand side of eq 18 is given by

$$\left(\frac{dN_i}{dt}\right)_{nucl} = \begin{cases} B_0, i = i_0 \\ 0, i \neq i_0 \end{cases}$$

To avoid problems with the numerical integration algorithm, it is convenient to assign the particles produced by nucleation to two contiguous classes:

$$\left(\frac{dN_i}{dt}\right)_{nucl} = \begin{cases} hB_0, i = i_0 \\ (1-h)B_0, i = i_0 + 1 \\ 0, i \neq i_0, i_0 + 1 \end{cases} \quad (22)$$

where h is equal to $(L^* - L_i)/(L_{i+1} - L_i)$.

Discretization for Growth. The objective is to develop a discretized equation capable of describing correctly the PSD and its moments. This point is rather crucial because the calculation of the mass balance (eq 11) requires the correct prediction of the total number, length, surface, and volume of particles, that is, all moments $m_0 - m_3$. Hounslow at al. [30] have proposed the expression

$$\left(\frac{dN_i}{dt}\right)_{growth} = \frac{G}{L_i}(aN_{i-1} + bN_i + cN_{i+1})$$

where a, b, and c are coefficients depending on the discretization step r (eq 20), which guarantee the exact calculation of the zero, first, and second moments. However, the third moment is affected by an error, which is not always tolerable, and moreover, the above expression holds for constant growth rate only. As a result, a new discretization method, capable of exactly calculating a generic number M of moments has been developed. The new approach considers an expression of the form

$$\left(\frac{dN_i}{dt}\right)_{growth} = \frac{1}{L_i}\sum_{k=1}^{M} a_k N_{i-k+1} G_{i-k+1} \qquad i \geq k \quad (23a)$$

where the growth rate G_i in the *i*th class is given by the corresponding mean size $\overline{L_i}$ according to eq 17. The coefficients a_k are determined by imposing that the moments 0 to $M - 1$ are correctly predicted and, for size-dependent growth rate, they result in (see Supporting Information)

$$\begin{cases} \sum_{k=1}^{M} a_k = \dfrac{2\ln r}{(r^2-1)} & j = 1 \\ \sum_{k=1}^{M} a_k r^{(k-1)(j-1)} = \dfrac{j(j+1)}{j-1}\left(\dfrac{r^{j-1}-1}{r^{j+1}-1}\right) & j = 0, 2, .., M-1 \end{cases} \quad (23b)$$

Most calculations in this study were performed using $M = 4$. This choice guarantees, by definition, the exact prediction of the first four moments and a satisfactory reconstruction of the final PSD if the number of classes is large enough. A problem of this discretization technique as well as of previous methods[30−32] is the tendency to produce oscillations and negative classes in the PSD, especially when nucleation is included in the PBE. Therefore, the PSD cannot be directly obtained from the population of the different classes, but it has to be reconstructed from the moments as described, for example, by Randolph and Larson.[29] However, this problem is beyond the scope of the present study, as the prediction of the moments is sufficient for the purpose of solving the mass balances and to describe the evolution of the average properties of the system.

Discretization for Aggregation. The discretized equation for the rate of change of particle number proposed by Lister et al.[31] has been adopted. For the aggregation kernel, two different models were tested. The first model corresponds to the constant aggregation kernel β_0. However, for submicron particles, the Brownian kernel,

$$\beta_{i,j} = \frac{2k_B T}{3\mu}(R_i + R_j)^2(R_i^{-1} + R_j^{-1})$$

where k_B is the Boltzmann constant, T is the temperature, and μ is the viscosity, is more appropriate.

2.5. Nucleation and Growth Equations. The classical theory of nucleation and growth from a supersaturated solution has been used to relate the nucleation rate B_0 (eq 22) and growth rate term G_0 (eq 17) to fundamental physical quantities such as temperature, surface tension, and diffusion coefficients.

Nucleation. Nucleation was broken down in two subprocesses: primary nucleation and secondary nucleation. In the first case, nucleation in the absence of pre-existing crystalline matter was considered, that is, homogeneous nucleation. The

(31) Lister, J. D.; Smit, D. J.; Hounslow, M. J. *AIChE J.* **1995**, *41*, 591.

(32) Kumar, S.; Ramkrishna, D. *Chem. Eng. Sci.* **1997**, *52*, 4659.

number of new embryos created per unit time and unit volume is given by[17,33]

$$B_{0,\mathrm{hom}} = \frac{2D}{d^5}\exp\left(-\frac{\Delta G^*_{\mathrm{hom}}}{k_\mathrm{B}T}\right) \tag{24}$$

where T is the temperature, D is the diffusion coefficient of the solute, $\Delta G^*_{\mathrm{hom}}$ is the Gibbs free energy barrier for homogeneous nucleation, and d can be approximated with the molecular diameter of the solute (taken here as the unit cell edge of $BaTiO_3$). $\Delta G^*_{\mathrm{hom}}$ can be written as

$$\Delta G^*_{\mathrm{hom}} = \frac{4}{27}\frac{{\epsilon_\mathrm{A}}^3}{{\epsilon_\mathrm{V}}^2}\frac{\nu^2\gamma^3}{{k_\mathrm{B}}^2T^2\ln^2(S)} \tag{25}$$

where ν is the volume of the growth unit (assimilated to one unit cell) and γ is the surface tension of the crystalline phase. Secondary nucleation as intended here corresponds to the creation of new three-dimensional embryos directly on the surface of the crystalline particles of $BaTiO_3$ already present in the suspension as a result of former nucleation and growth events and can be considered as a special case of heterogeneous nucleation. As for homogeneous nucleation, for secondary nucleation, the number of nuclei created per unit time and unit volume of the suspension is[34]

$$B_{0,\mathrm{sec}} = \frac{2D}{d^4}\exp\left(-\frac{\Delta G^*_{\mathrm{sec}}}{k_\mathrm{B}T}\right)x_\mathrm{A}A_\mathrm{T} \tag{26}$$

where x_A is the fraction of the overall particle surface A_T available for secondary nucleation. For a discretized PSD, using definition 15c, the overall particle surface per unit volume results from

$$A_\mathrm{T} = \epsilon_\mathrm{A}F_\mathrm{A}\sum_j N_jL_j^2 \tag{27}$$

where F_A is the ratio $\overline{L_i^2}/L_i^2$ given by eq 21. The Gibbs free energy barrier for secondary nucleation can be written as

$$\Delta G^*_{\mathrm{sec}} = \frac{4}{27}\frac{{\epsilon_\mathrm{A}}^3}{{\epsilon_\mathrm{V}}^2}\frac{\nu^2{\gamma_\mathrm{eq}}^3}{{k_\mathrm{B}}^2T^2\ln^2(S)} \tag{28}$$

where γ_{eq} is a function of the geometry of the embryo and of the energy of adhesion σ of the embryo on the substrate. For the simplest case of a cubic embryo

$$\gamma_{\mathrm{eq}} = \frac{\gamma}{6}\left(6 - \frac{\sigma}{\gamma}\right) \tag{29}$$

The value of σ is constrained in the range $0-2\gamma$. The case $\sigma = 0$ corresponds to the absence of a substrate, that is, homogeneous nucleation, whereas for $\sigma = 2\gamma$, perfect epitaxial growth occurs. For $\sigma > 0$, there is a net surface energy gain when nucleation occurs on the substrate, $\gamma_{\mathrm{eq}} < \gamma$, and the free energy barrier is lowered in comparison to homogeneous nucleation. Consequently, secondary nucleation can proceed even at relatively low values of supersaturation when homogeneous nucleation has almost arrested. The overall nucleation rate $\hat{B}$, which appears in the mass balances (eqs 11 and 12), has units of mol cm^{-3} s^{-1}, and therefore,

$$\hat{B} = B_0\frac{v_\mathrm{e}}{V_\mathrm{m}} \tag{30}$$

where v_e is the volume of the embryo and V_m is the molar volume of $BaTiO_3$. For a given supersaturation, the critical size for homogeneous nucleation will be different from that of secondary nucleation and, in general, new particles can appear in different classes i_0 and k_0. The volume of the embryo can be defined as (eq 15d)

$$v_{\mathrm{e},i} = \epsilon_\mathrm{V}F_\mathrm{V}{L_i}^3 \tag{31}$$

where F_V is the ratio $\overline{L_i^3}/L_i^3$ (eq 21). When eqs 22 and 31 are applied, eq 30 can be rewritten as

$$\hat{B} = \frac{\epsilon_\mathrm{V}F_\mathrm{V}}{V_\mathrm{m}}\{B_{0,\mathrm{hom}}[h_{\mathrm{hom}}{L_{i_0}}^3 + (1-h_{\mathrm{hom}}){L_{i_0+1}}^3] + B_{0,\mathrm{sec}}[h_{\mathrm{sec}}{L_{k_0}}^3 + (1-h_{\mathrm{sec}})L_{k_0+1}{}^3)] \tag{32}$$

Growth. When the classic approach for multicomponent diffusion is followed,[33] with reference to reaction 2 and to the species $Ti(OH)_4$, the growth rate of particles in the ith class (eq 17) is

$$G_i = \frac{\mathrm{d}L_i}{\mathrm{d}t} = \frac{G_0}{L_i} = 2V_\mathrm{m}J_{\mathrm{Ti(OH)_4}}\frac{4k_DV_\mathrm{m}D}{F_LL_i}([\mathrm{Ti(OH)_4}] - [\mathrm{Ti(OH)_4}]_{\mathrm{surf}}) \tag{33}$$

where $J_{\mathrm{Ti(OH)_4}}$ is the diffusive flux, $[\mathrm{Ti(OH)_4}]_{\mathrm{surf}}$ is the concentration at the surface of the growing particles, D is the diffusion coefficient, and k_D is the growth correction factor. The physical meaning of k_D will be discussed later. The term $[\mathrm{Ti(OH)_4}]_{\mathrm{surf}}$ can be obtained by assuming local equilibrium conditions and similar diffusion coefficients for the diffusing species, as shown in ref 33. Moreover, as OH^- is present in a large excess in comparison to the stoichiometric amount required by reaction 1, the concentration of hydroxyl ions at the surface of the growing particle was taken to be equal to the bulk concentration. Therefore, it results in

$$2[\mathrm{Ti(OH)_4}]_{\mathrm{surf}} = ([\mathrm{Ba_{aq}}] - [\mathrm{Ti(OH)_4}]) + \sqrt{([\mathrm{Ti(OH)_4}] - [\mathrm{Ba_{aq}}])^2 + 4\frac{K_\mathrm{s}(1+K_1[\mathrm{OH^-}])}{[\mathrm{OH^-}]^2}} \tag{34}$$

where the overall concentration of dissolved barium has been considered. The growth rate $\hat{G}$, which appears in mass balances 11 and 12, has units of mol cm^{-3} s^{-1}, and therefore, from the definition (15d) of moment m_3 we have

$$\hat{G} = \frac{\epsilon_\mathrm{V}}{V_\mathrm{m}}\frac{\mathrm{d}m_3}{\mathrm{d}t} \tag{35}$$

and substituting from eq 16c, this gives

(33) Nielsen, A. E. *Kinetics of Precipitation*; Pergamon: Oxford, U. K., 1964.
(34) Kern, R.; Le Lay, G.; Métois, J. J. In *Current Topics in Materials Science*; Kaldis, E., Ed.; North-Holland: Amsterdam, Netherlands, 1979; Vol. 3, p. 135.

$$\hat{G} = \frac{3\epsilon_V G_0 m_1}{V_m} \tag{36}$$

By combining eqs 19 and 36, the final expression of the growth rate is

$$\hat{G} = \frac{3\epsilon_V F_L G_0}{V_m} \sum_i N_i L_i \tag{37}$$

3. Results and Discussion

The number of equations required to predict the evolution of the average particle size with time is determined by the number of moments that need to be correctly predicted and by the size range of particles to be modeled. For $BaTiO_3$, the smallest particles correspond to the size of the critical nuclei, 2−3 nm. The largest crystals detected in the experiments were on the order of a few hundred nm. Therefore, q in eq 20 was set to 1, resulting in 20−25 equations analogous to eq 18. This choice guarantees the exact calculation of moments m_0 to m_3, a small error on moment m_4, and that the nucleation process is well-represented. The discretized population balance equations and eqs 7, 11, and 12 related to the mass balances were then simultaneously solved using the LSODE[35] integration routine, which is particularly suitable for stiff systems of first-order ordinary differential equations, as found here. LSODE makes use of the backward differentiation formulas. The optimal value of the adjustable model parameters was found by using a nonlinear fitting approach, as discussed in the following section.

A meaningful model for the precipitation of $BaTiO_3$ has to correctly reproduce (1) the sigmoidal shape of the fractional reactant conversion versus time curves and (2) the polycrystalline morphology of the particles. This feature, evident from electron microscopy observations (Figure 1), was confirmed by measurements of specific surface area and crystallite size.[25] Formation of polycrystalline particles during solution precipitation or mild hydrothermal synthesis of $BaTiO_3$ has been reported by several authors.[3,8,22,24,27,36] Initially, primary nucleation, growth, and aggregation were included in the model, as it is customary in modeling precipitation processes (see, for example, ref 37). However, any attempts to reasonably fit the experimental kinetic data (see Figure 2 as an example) failed. If the model is forced to reproduce the initial low reaction rate (up to 20% conversion), the subsequent strong increase of the reaction rate cannot be accounted for (curve 1 in Figure 2). On the contrary, if the model is constrained to give the correct reaction rate at half-transformation, the overall kinetics is too fast (curve 2 in Figure 2). A trivial solution would consist of introducing a convenient induction time (≈950 s in the example of Figure 2) to shift the kinetic curve in the right position. This approach has two main drawbacks. First, induction times of minutes to tens of minutes cannot be justified on a theoretical basis for the system under consideration.[17] Second, nucleation and growth of $BaTiO_3$ nanocrystals was clearly observed by electron microscopy in the whole time interval from 240−900 s, that is, when conversion is < 1%.[25] The above difficulties and contradictions were overcome by including secondary nucleation in the model. Secondary nucleation readily explains the acceleration of the reaction kinetics, and moreover, it directly accounts for the polycrystalline nature of the final particles. As a result, an aggregative mechanism is no longer required to explain the generation of polycrystalline particles. It is assumed that every $BaTiO_3$ nanocrystal resulting from a primary nucleation event leads to a distinct polycrystalline particle by a succession of secondary nucleation events and growth. Therefore, the number of crystallites per particle will increase with the age of the particle until the secondary nucleation rate becomes null. If dissolution of the smallest particles due to Ostwald-like ripening processes may be neglected, the overall number of primary nuclei will be equal to the final number of particles N_p, whereas the overall number of secondary nuclei will be given by $N_c - N_p$, where N_c is the final number of elementary crystallites. The two quantities can be easily calculated from the mean crystallite size d_c

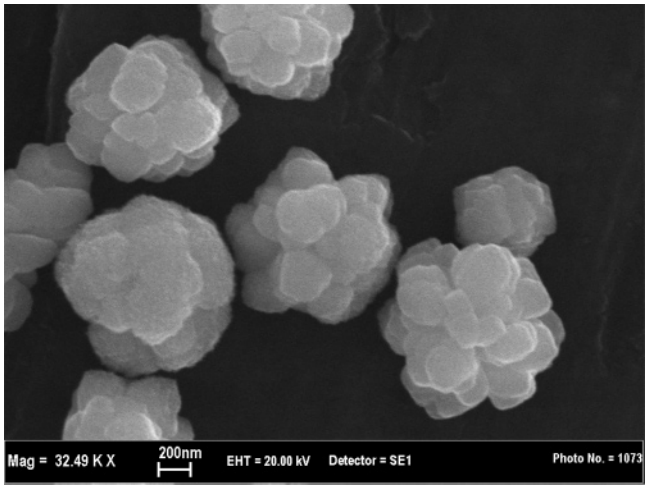

Figure 1. Morphology of $BaTiO_3$ particles precipitated at 82 °C, [Ba] = 0.044 mol dm^{-3}, and $R = 1.11$. Bar: 200 nm.

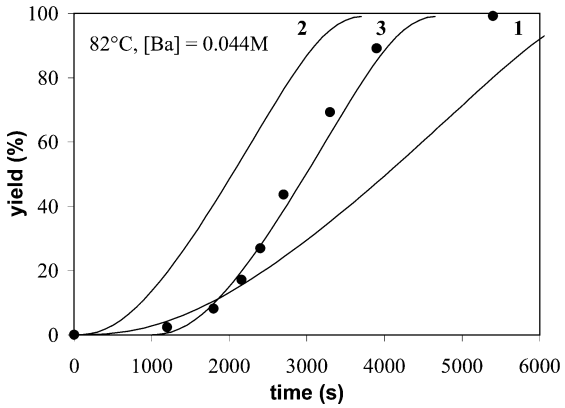

Figure 2. Comparison between the experimental formation kinetics of $BaTiO_3$ (82 °C, [Ba] = 0.044 mol dm^{-3}) and different models incorporating primary nucleation and growth. Curve 1 is forced to reproduce the initial low reaction rate. Curve 2 gives the same reaction rate at half-transformation as the experimental data. Curve 3 is the same as curve 2, but shifted by 950 s.

(35) Hindmarsh, A. C. Odepack, a Systematized Collection of Ode Solvers. In *Scientific Computing*; Stepleman, R. S., Ed.; North-Holland: Amsterdam, Netherlands, 1983; pp 55−64.
(36) Zhao, L.; Chien, A. T.; Lange, F. F.; Speck, J. S. *J. Mater. Res.* **1996**, *11*, 1325.
(37) Zauner, R.; Jones, A. G. *Chem. Eng. Sci.* **2000**, *55*, 4219.

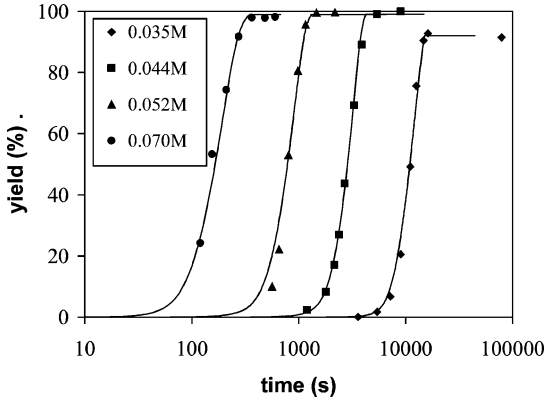

Figure 3. Comparison between the experimental formation kinetics of $BaTiO_3$ at 82 °C (symbols) and the predictions of the model (solid curves). The legend indicates the barium concentration.

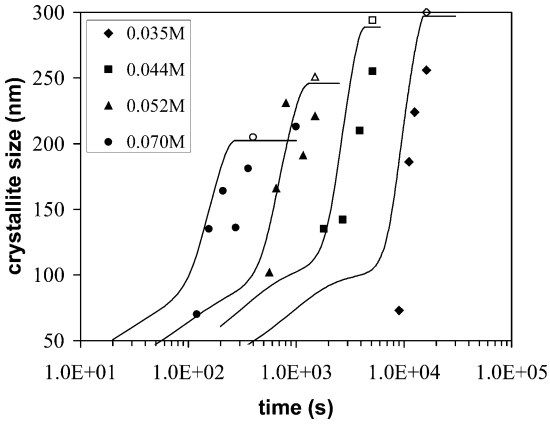

Figure 4. Growth of the elementary $BaTiO_3$ crystals at 82 °C. Full symbols: crystallite size estimated from XRD measurements. Open symbols: crystallite size calculated from specific surface area. Solid lines: model. The legend indicates the barium concentration.

and the mean particle diameter d_p measured on the final powder knowing the overall titanium concentration. The ratio N_c/N_p corresponds to the final average number of crystallites per particle. Optimized values of the adjustable model parameters were then obtained by fitting the experimental values of N_p, N_c, d_p, and d_c corresponding to the final yield and the fractional conversion versus time data. The model was successfully applied to eight sets of kinetic data collected in different conditions of concentration and temperature.[25] The comparison between the experimental kinetic data collected at 82 °C and the model is shown in Figure 3. Similar good agreement is also obtained for the data collected at 92 °C. The evolution of the size of the elementary crystals (Figure 4) is reasonably reproduced by the model. The presence of two nucleation processes, primary and secondary nucleation, is evident from the calculated growth curves, where a sudden change of their slope is observed. Finally, the growth of the polycrystalline particles at 82 °C is illustrated in Figure 5.

The adjustable model parameters are (1) γ, the surface energy of $BaTiO_3$ in the suspension (eq 25); (2) γ_{eq}, the equivalent surface energy involved in the formation of critical three-dimensional secondary nuclei on the $BaTiO_3$ surface (eq 28); (3) K_s, the solubility product of $BaTiO_3$ (eq 4); (4) k, the rate constant for THG dissolution (eq 7); and (5) k_D, the growth correction factor (eq 33). The equilibrium constant

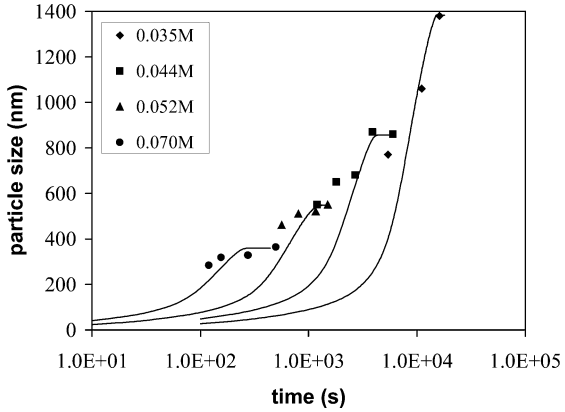

Figure 5. Growth of the polycrystalline $BaTiO_3$ particles at 82 °C. Full symbols: mean size from particle size distribution. Solid lines: model. The legend indicates the barium concentration.

of reaction 3 was obtained from the thermodynamic data reported by Lencka and Riman.[16] Supersaturation is computed by means of eq 4 using the constant K_s and the current concentration of the aqueous species Ba^{2+}, $Ti(OH)_4$, and OH^-. The relatively high initial values of the supersaturation (3000−5000, see Table 1) provides a posteriori justification of having considered primary nucleation as homogeneous and growth-governed by diffusion. The $Ti(OH)_4$ concentration in the suspension is determined by the dissolution of THG (reaction 5) and controlled by the equilibrium constant K/K_s and the rate constant k (eq 7). The value of K/K_s defines the maximum value of $[Ti(OH)_4]$, that is, the solubility of THG. For a given temperature, the rate of primary nucleation is determined by supersaturation and by the surface energy γ (eqs 24 and 25). Likewise, γ_{eq} or, equivalently, σ decides the value of B_{sec} (eqs 26 and 28). The reaction rate at half-transformation is mainly related to the growth rate of the elementary crystallites and, therefore, determined by the diffusion coefficient D (eq 33). The curvature of the yield versus time curves above 50% conversion is further affected by the rate of THG dissolution through the kinetic constant k (eq 7). The lower the value of k, the more gradual the change in slope.

The optimized value of the adjustable parameters of the model are reported in Table 1 for each investigated experimental condition. For a given temperature, 82 or 92 °C, the parameters γ, γ_{eq}, and K_s take values nearly independent of concentration with variations ≤ 1.5%. We are not aware of any experimental data of the surface tension of $BaTiO_3$ in water. However, γ can be estimated to be ≈0.22 J m^{-2} on the basis of the Gibbs adsorption isotherm[38] and ≈0.15 J m^{-2} from an empirical relationship that correlates the surface tension of oxides with their solubility in water.[39] The present kinetic model gives ≈0.19 J m^{-2}, a value consistent with the above estimates. The optimized value of γ_{eq} is ≈0.17 J m^{-2}, which determines a net surface energy gain in comparison to primary homogeneous nucleation. For a cubic nucleus, the energy of adhesion corresponding to the values of γ_{eq} reported in Table 1 is ≈0.14 J m^{-2}. This figure

(38) Mersmann, A. *J. Cryst. Growth* **1990**, *102*, 841.
(39) Sonhel, O.; Garside, J. *Precipitation: Basic Principles and Industrial Applications*; Butterworth & Heinemann: Oxford, U. K., 1992; pp 37−39.

Table 1. Reaction Conditions and Adjustable Model Parameters[a]

expt	[Ba] (mol dm^{-3})	S ($t = 0$)	γ (J m^{-2})	γ_{eq} (J m^{-2})	σ^b (J m^{-2})	K_s (mol^4 dm^{-12})	k (dm^3 mol^{-1} s^{-1})	k_D
				82 °C				
1	0.035	2900	0.190	0.167	0.141	4.83×10^{-13}	1.0×10^{-3}	0.049
2	0.044	3790	0.191	0.169	0.132	4.82×10^{-13}	6.0×10^{-3}	0.25
3	0.052	4730	0.191	0.170	0.128	4.84×10^{-13}	1.3×10^{-2}	0.35
4	0.070	6790	0.193	0.171	0.129	4.82×10^{-13}	8.2×10^{-2}	1.0
			0.191 (0.0012)	*0.169 (0.0017)*	*0.133 (0.0059)*	*4.83(0.01) × 10^{-13}*		
				92 °C				
5	0.023	2720	0.194	0.168	0.156	2.35×10^{-13}	1.0×10^{-3}	0.23
6	0.029	3480	0.192	0.167	0.152	2.27×10^{-13}	6.5×10^{-3}	1.0
7	0.035	4250	0.195	0.171	0.141	2.34×10^{-13}	2.0×10^{-2}	1.0
8	0.0405	5130	0.196	0.172	0.143	2.32×10^{-13}	5.0×10^{-2}	1.0
			0.194 (0.0017)	*0.170 (0.0024)*	*0.148 (0.0072)*	*2.32(0.04) × 10^{-13}*		

[a] See text for symbols. Mean values are indicated in italics. Values in parentheses denote the standard deviation. [b] Computed for a cubic nucleus

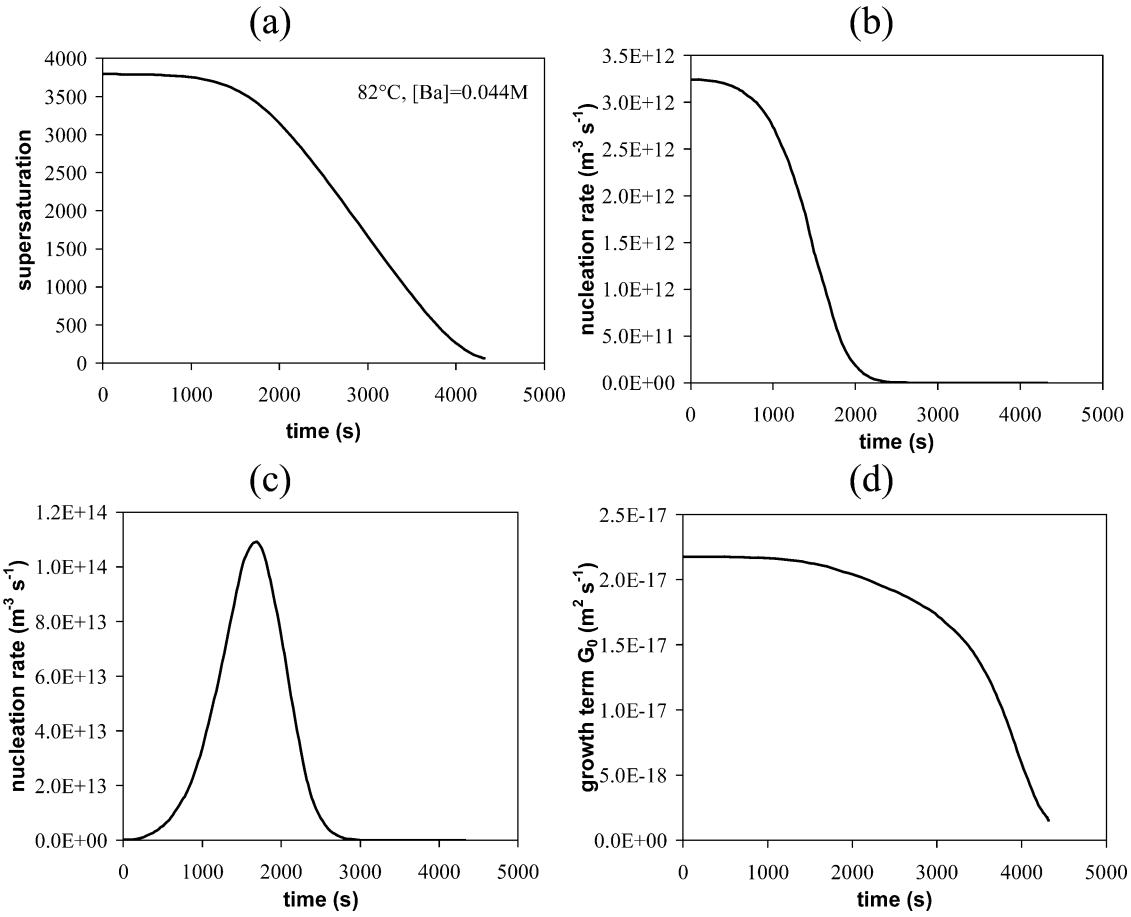

Figure 6. Evolution of some fundamental quantities during the formation of $BaTiO_3$ at 82 °C and [Ba] = 0.044 mol dm^{-3}. (a) Supersaturation. (b) Primary nucleation rate. (c) Secondary nucleation rate. (d) Growth term G_0 (eq 33).

represents about 37% of 2γ, the theoretical maximum value attainable by σ. The equilibrium solubility of the THG phase (see reaction 5) can be calculated from K/K_s and gives, taking [OH^-] = 1 mol dm^{-3}, $\approx 3.5 \times 10^{-7}$ mol dm^{-3} at 82 °C and $\approx 2.1 \times 10^{-7}$ mol dm^{-3} at 92 °C. These values can be compared with the solubility of anatase and rutile at 90 °C calculated by Eckert et al.,[22] 7.5×10^{-8} and 7.1×10^{-9} mol dm^{-3}, respectively. Thus, THG is 3−5 times more soluble than the anatase phase. At 92 °C, the value of K_s provided by the model is 2.4×10^{-13} mol^4 dm^{-12}, corresponding to a standard Gibbs free energy $\Delta G°_s$ of 88 kJ mol^{-1}. The combination of the standard free energies of formation [16] of the different species in reaction 2 gives $\Delta G°_s = 109$ kJ mole^{-1} and a solubility product of 2.6×10^{-16} mol^4 dm^{-12}. A 20% difference in the free energy is considerable but still acceptable if the errors on the thermodynamic data and the approximations of the present model are taken into account. From the experimental solubility data reported by Pinceloup et al.,[11] it can be estimated that K_s ranges from 5×10^{-16} to 1×10^{-14} mol^4 dm^{-12} at room temperature, again consistent with the present kinetic model.

The evolution of supersaturation and of the rate of the elementary processes of primary nucleation, secondary nucleation, and growth with time at 82 °C and [Ba] = 0.044 mol dm^{-3} (expt #2) is reported in Figure 6. Supersaturation (Figure 6a) is nearly constant up to 1500 s because of the small precipitated fraction (Figure 2) and then progressively decreases. The maximum value of the primary nucleation

rate (Figure 6b) corresponds to $t = 0$, that is, the highest supersaturation. The highest rate of secondary nucleation (Figure 6c) occurs after ≈1700 s (10% yield) and is still significant after ≈2500 s (≈30% yield), when primary nucleation has stopped. After ≈3000 s (≈50% yield), growth becomes the predominant process. This behavior can be explained as follows. At the very beginning, primary nucleation provides supercritical nuclei that grow further. As the rate of secondary nucleation is proportional to the overall surface of the particles (eq 26), it will increase with time such as in a self-catalytic process. At a later time, the lowering of supersaturation induces a decrease of the secondary nucleation rate and growth will become predominant. Experimentally, it was observed that the number density of particles no longer increases once the converted fraction exceeds 40−60%,[25] and this indicates a negligible contribution of nucleation beyond that limit, in agreement with the prediction of the model. The rapid drop of the growth term G_0 for times longer than 3500 s (Figure 6d) is related to the decrease of the concentration difference term in eq 33 when reaction approaches complete conversion. The concentration of $Ti(OH)_4$ in the aqueous phase (eq 11) remains relatively close to the equilibrium value (variation within 30%) determined by the equilibrium constant K_s/K until the yield attains 70−80%, because the THG phase acts as a buffer for the supply of $Ti(OH)_4$. Beyond this limit, the amount of hydrous titania is strongly reduced and the concentration of $Ti(OH)_4$ starts to decrease rapidly, and its value is mainly determined by the kinetic constant k. The value of k (Table 1) is very sensitive to the initial supersaturation. Apparently, THG dissolution is faster at higher barium concentrations.

The diffusion coefficient of $Ti(OH)_4$ at 80−90 °C was estimated to be $\approx 3 \times 10^{-9}$ m^2 s^{-1}. Using this value, the growth rate in four of the eight experiments could be successfully reproduced. However, for the experiments conducted at lower concentrations (see Table 1), the growth rate is apparently lower than that predicted from the above value of D and the introduction of the growth correction factor k_D was required (eq 33). The product Dk_D can then be described as an effective diffusion coefficient. Except for expt #1, the correction is not very large, and the product Dk_D is $(0.7-1.1) \times 10^{-9}$ m^2 s^{-1}. Although its physical meaning is not completely clear, most likely, k_D compensates for some deficiencies of the model in describing the growth of polycrystalline particles. In particular, the elementary crystallites were considered to be growing as they were not interacting. This is a direct consequence of the fact that the PBE has only one internal coordinate, that is, the size of the elementary crystallites. In contrast, the crystallites are part of a larger polycrystalline particle. It is quite likely that the crystals at the surface grow faster than the crystals in the interior even though, according to BET measurements,[25] the solvent has access to a fraction of the inner surfaces of the particle. The lower the concentration, the bigger the particles and the larger the number of crystallites per particle. For instance, at 82 °C, it is $N_c/N_p \approx 100$ when [Ba] = 0.035 mol dm^{-3} (expt #1, $k_D = 0.05$) and $N_c/N_p \approx 6$ when [Ba] = 0.07 mol dm^{-3} (expt #4, $k_D = 1$). As a result, crystallites that are part of large particles grow, on average, at a lower rate than crystallites in small particles, and a factor $k_D < 1$ compensates for this effect. A further effect that is not explicitly included in the model is the recrystallization of the particles induced by Ostwald-like ripening processes. Experimentally, a significant decrease of the number density of particles for fractional conversion >50% has been observed[25] for the synthesis carried out at the lowest concentration at both temperatures (expts #1 and #5). Under these conditions, recrystallization can become important because the time needed to attain the final yield is on the order of hours.

The growth of spherical- or even polygonal/polyhedral-shaped particles by aggregation of smaller particles is the process usually invoked to explain the generation of polycrystalline particles.[17,28] When the elementary crystallites aggregate along well-defined crystallographic orientations (oriented attachment, epitaxial aggregation), the result is a single crystal-like particle.[40−42] Secondary nucleation can represent an alternative or concurrent mechanism to aggregation of small particles. The adhesion energy of the secondary nucleus on the substrate surface represents a driving force for the growth of polycrystalline particles with some degree of order. The higher the adhesion energy, the more oriented the particles in the final structure. As a result, secondary nucleation might be a rather common mechanism involved in the growth of particles or systems characterized by a substructure and some level of self-organization.

4. Summary and Conclusions

A general kinetic model for the aqueous synthesis (solution precipitation and hydrothermal synthesis) of barium titanate particles has been developed. The model can be applied to all systems where a titanium hydroxide gel is used as a precursor or formed as an intermediate product. The classical theory of nucleation and growth from supersaturated solutions has been used to relate the nucleation rate and the growth rate to fundamental physical quantities such as temperature, surface tension of the solid phase, and diffusion coefficient. The evolution of the system (crystal size vs time, yield vs time) has been described by means of mass and population balance equations. The resolution of the PBEs has been carried out using the class method. This corresponds to replacing the continuous particle distribution with a discretized distribution consisting of a limited number of classes. The total number, length, surface, and volume of the particles were obtained from the moments of the discretized PSD, following the approach of Randolph and Larson.[29] The model was successfully applied to eight sets of kinetic data collected at different temperatures and concentrations. The optimized values of the adjustable parameters of the model—the solubility product of $BaTiO_3$, the surface tension of $BaTiO_3$, the equivalent surface energy

(40) (a) Penn, R. L.; Banfield, J. F. *Science* **1998**, *281*, 969. (b) Banfield, J. F.; Welch, S. A.; Zhang, H. Z.; Ebert, T. T.; Penn, R. L. *Science* **2000**, *289*, 751.
(41) Jongen, N.; Bowen, P.; Lemaitre, J.; Valmalette, J. C.; Hofmann, H. *J. Colloid Interface Sci.* **2000**, 226, 189.
(42) Penn, R. L.; Oskam, G.; Strathmann, T. J.; Searson, P. C.; Stone, A. T.; Veblen, D. R. *J. Phys. Chem. B.* **2001**, *105*, 2177.

involved in the formation of critical secondary nuclei on the $BaTiO_3$ surface, and the kinetic constant for dissolution of the titanium hydroxide precursor—showed good agreement with the best estimates available.

Nucleation was broken down in two subprocesses: primary homogeneous nucleation and secondary nucleation. Secondary nucleation is defined as the creation of new, three-dimensional embryos directly on the surface of crystalline $BaTiO_3$ particles already present in the suspension as a result of former nucleation and growth events. Secondary nucleation can readily explain the rapid increase of the $BaTiO_3$ formation rate after an initial period dominated by primary nucleation. Moreover, secondary nucleation can account for the polycrystalline nature of the final particles. It is assumed that every $BaTiO_3$ nanocrystal resulting from a primary nucleation event leads to a distinct polycrystalline particle by a succession of secondary nucleation events and growth. As a result, an aggregative mechanism is no longer required to explain the generation of polycrystalline particles.

Diffusion-controlled growth was assumed to be the predominant process involved in the coarsening of the elementary crystals that compose the polycrystalline particles. This was opportunely taken into account in the model using a modified growth algorithm in comparison to existing literature.[29−31] The new algorithm was capable of exactly calculating a generic number of moments. The elementary crystals were considered to be growing as they were noninteracting, rather than being part of a larger structure. This is a crude approximation but avoids the introduction of completely empirical relationships between growth rate and supersaturation. The problem was corrected, at least in part, by introducing a multiplicative growth correction factor in the expression of the growth rate. This factor is significantly different from unity only for large particles composed of more than some tens of elementary crystals.

More generally, the main limitation of the present approach is the use of PBEs with only one internal coordinate, that is, the size of the elementary crystallites. A more rigorous approach would consist of the use of PBEs with at least two internal coordinates, for example, the size of the primary crystals and the size of the polycrystalline particles. In this way, it should be possible to better describe whether the interactions between the elementary crystallites affect the overall precipitation process. However, the application of PBEs with more than one internal coordinate to precipitation problems is still at an early stage of development.

Finally, caution should be exercised in applying the proposed model to diverse systems and experimental situations. Extrapolation of the present results to very different temperature and concentration conditions will lead to erroneous conclusions if the reaction mechanism changes. Moreover, the model assumes that the system is well-mixed and that the precipitation rate is uniquely controlled by the chemical kinetics. While these assumptions are generally valid in small-scale laboratory reactors, they may fail in larger industrial plants where mixing is slower and less efficient. A mixing-limited precipitation rate is one of the problems commonly encountered in the scale-up of precipitation processes.

Acknowledgment. This work has been supported, in part, by the European Community under the "Competitive and Sustainable Growth" Program (Contract No. G5RD-CT-1999-00123). We thank Prof. P. Bowen, EPFL, Lausanne, Switzerland, for helpful discussions.

Supporting Information Available: Proofs of eqs 16c and 23b. This material is available free of charge via the Internet at http://pubs.acs.org.

CM051119F